Received: 16 August 2023 | Revised: 10 April 2024 | Accepted: 18 May 2024

DOI: 10.1002/met.2218

Meteorological Applications
Science and Technology for Weather and Climate
Open Access
RMetS

RESEARCH ARTICLE

Application of commercial microwave links (CMLs) attenuation for quantitative estimation of precipitation

Magdalena Pasierb[1] | **Zofia Bałdysz**[1] | **Jan Szturc**[1] | **Grzegorz Nykiel**[1,2] | **Anna Jurczyk**[1] | **Katarzyna Ośródka**[1] | **Mariusz Figurski**[1] | **Marcin Wojtczak**[3] | **Cezary Wojtkowski**[3]

[1]Institute of Meteorology and Water Management - National Research Institute, Warsaw, Poland

[2]Faculty of Civil and Environmental Engineering, Gdansk University of Technology, Gdansk, Poland

[3]NetWorkS! Sp. z o.o, Warszawa, Poland

Correspondence
Magdalena Pasierb, Institute of Meteorology and Water Management – National Research Institute, PL 01-673 Warszawa, Poland.
Email: magdalena.pasierb@imgw.pl

Abstract

Precipitation estimation models are typically sourced by rain gauges, weather radars and satellite observations. A relatively new technique of precipitation estimation relies on the network of Commercial Microwave Links (CMLs) employed for cellular communication networks: the rain-inducted attenuation in the links enables the precipitation estimation. In the paper, it is analysed to what extent the precipitation derived from CML attenuation data is useful in estimation of the precipitation field with the high temporal and spatial resolution required in nowcasting models. Two methods of determination of precipitation along CMLs from attenuation of signal with several frequencies were proposed. Then, in order to generate precipitation field, three approaches for assigning appropriate precipitation values to a specific point or set of pixels along the link are developed and tested. The CML-based estimates are compared with point observations from manual rain gauges and multi-source precipitation fields using daily and half-hourly accumulations. It was found that the CML-based precipitation fields are much worse than radar-derived estimates. At the same time, they had slightly poorer reliability than spatially interpolated telemetric rain gauge data and significantly higher reliability than satellite estimates. Furthermore, the impact of link characteristics, such as length and frequency, on the reliability of CML-based precipitation estimates is analysed.

KEYWORDS

CML, commercial microwave links, precipitation estimation

1 | INTRODUCTION

Intense precipitation causing flash floods is one of the most dangerous natural weather hazards, resulting in life-threatening and economic losses (Cornwall, 2016; Herring et al., 2018; Sokol et al., 2021). Due to global warming, extreme precipitation is likely to be more intense and frequent (Seneviratne et al., 2012) and becomes an increasing challenge for numerical weather prediction models, especially for nowcasting models,

which typically provide forecasts up to 2–6 h ahead. Since mitigating actions strongly depend on the forecasts of the amount and spatial distribution of the precipitation field (Wilson et al., 2010), reliable quantitative estimations and short-term predictions are crucial.

Precipitation estimation models are typically sourced by rain gauges (telemetric and manual), ground weather radars (including local area devices), radars on board meteorological satellites in low earth orbits and satellite-based imagers and sounders placed on satellites in polar and geostationary orbits. All these observations are affected by many measurement errors, so they must be subjected to advanced quality control. Due to the very different structure of measurement errors associated with different techniques, these data are complementary, so a common approach for precipitation estimation is to merge data from various sources. The high expectations of the data users regarding the data quality and resolution lead to the investigation of the usefulness of new, opportunistic sources of precipitation information, such as measurements with private rain gauges or attenuation data in microwave links. Applying such new data sources hopefully will allow increasing the reliability of precipitation estimates and, consequently, the precipitation forecasts, especially the nowcasts.

A technique of precipitation estimation that relies on the network of Commercial Microwave Links (CMLs) employed for cellular communication networks has recently been increasingly studied (Leijnse et al., 2007; Messer, 2007; Messer & Sendik, 2015; Rahimi et al., 2003; Uijlenhoet et al., 2018; Upton et al., 2005). Typically, CML networks operate at frequencies between 5 and 40 GHz, although they may reach up to 80 GHz. Within these frequencies, rainfall causes attenuation of electromagnetic wave propagation on the path between two antennas. This signal path loss can be detected and converted into rain rate along the CML path, using power law (Atlas & Ulbrich, 1977; Olsen et al., 1978). Depending on the frequency, the relation between rain-inducted attenuation and rain rates varies, with high frequencies showing higher attenuation for the same amount of rain (Chwala & Kunstmann, 2019), while the E-band (71–76 and 81–86 GHz) also enables the estimation of near-surface humidity (David et al., 2009; Fencl et al., 2020, 2021).

The constantly increasing number of CML infrastructure enables for using rain rate along paths in reconstructing rainfall fields. These fields can have regional (Chwala et al., 2012; Rios Gaona et al., 2018; Roversi et al., 2020) and country-wide scales (de Vos et al., 2019; Graf et al., 2020, 2021; Overeem et al., 2013, 2016a), while a significantly higher density of CMLs in an urbanized area also allows for more detailed analysis, like rainfall-runoff modelling (Pastorek et al., 2023). Next to the fairly high spatial distribution of the CML links, the advantage of CML-delivered precipitation products also comes from the very high temporal resolution of rain rates, which may reach even a 1-min interval (Graf et al., 2020). Additionally, the CML rainfall performance may be better represented when previously CML links are adjusted by rain gauges (Fencl et al., 2017) or by performing calibration of parameters used in rainfall retrieval algorithms (Wolff et al., 2022). A comprehensive description of CML rainfall estimation was given by Chwala and Kunstmann (2019) and Uijlenhoet et al. (2018).

The aim of this paper is the assessment of the reliability of the precipitation derived from CML attenuation data, especially in terms of the multi-source precipitation estimation with the high temporal and spatial resolution required in nowcasting models and rainfall-runoff models for flash-flood forecasting. The CML rainfall was estimated independently for each of the analysed links, using differences between transmitted and received signal levels with dry/wet classification. Since analysed links have several sublinks operating at different frequencies for which such a procedure was used, two methods were tested for the determination of the final precipitation value. In next step, different approaches for assigning appropriate precipitation values to a specific point or set of pixels along the link are developed and tested to generate a precipitation field. Finally, the CML-based estimates were compared with point observations from manual rain gauges performed once a day and multi-source precipitation fields using half-hourly and daily accumulations.

The paper is structured as follows: Chapter 2 discusses the different precipitation data used for the analyses, and the methodology for generating CML-based precipitation data is described in Chapter 3. Chapter 4 evaluates the results of assessing the data reliability compared with different precipitation fields, including multi-source ones, as well as point observations from manual rain gauges. In Chapter 5, an influence of link characteristics on reliability of precipitation estimates is analysed and examples of applying of the CML-based precipitation are presented. Final Chapter 6 summarises the results and provides suggestions for further work.

2 | DATA

Various types of precipitation data from July 19 to August 18, 2022 have been used in this study. The data analysed here are precipitation estimates generated from attenuation data in CMLs (*CML*). They are verified by

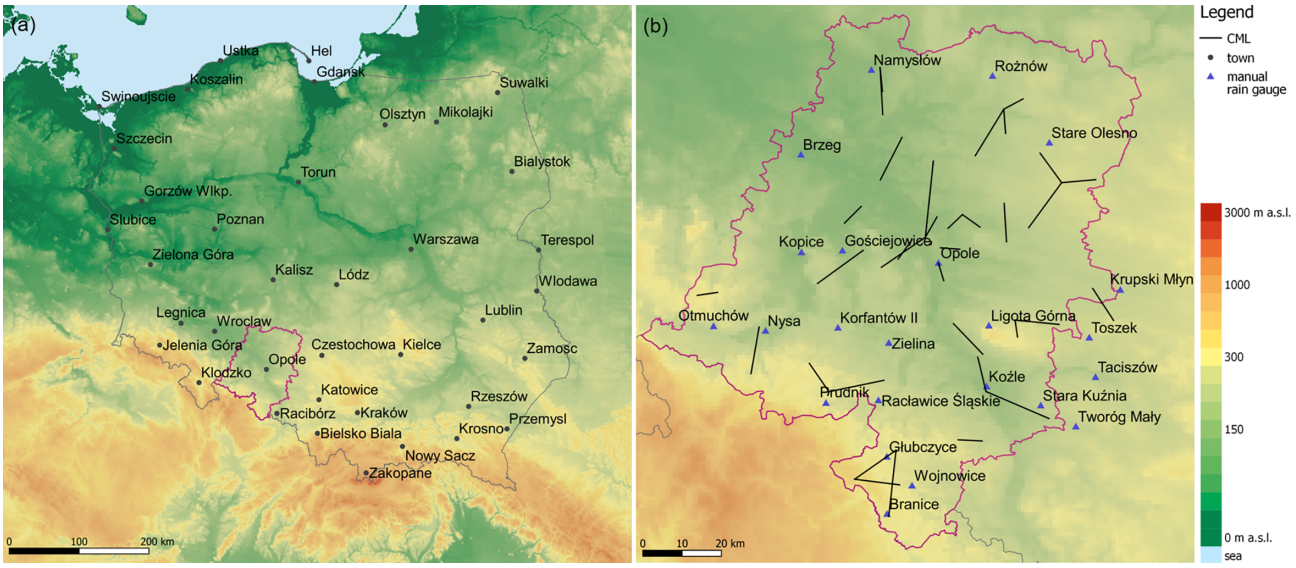

FIGURE 1 Study area (Opole Voivodeship) marked with pink borders (a); locations of CMLs and manual rain gauges (b).

independent measurements from (i) manual rain gauges and (ii) multi-source estimates (*GRS*) calculated from data provided by the telemetric rain gauges (G_{int}), weather radars (R_{cor}) and meteorological satellite (S). Statistics of the CML-based precipitation was also compared with statistics obtained for the particular observation data G_{int}, R_{cor} and S.

2.1 | Study area

The area for which CML data were available includes the Opole Voivodeship (administrative region), which is located in southern Poland and borders the Czech Republic to the south (Figure 1a). This area is historically a part of Upper Silesia and covers an area of approximately 9500 km^2. The topography of the region is predominantly flat; only in the southern part, it is slightly mountainous.

Like the rest of Poland, the voivodship lies in a temperate climate zone, with a predominance of oceanic air influences. Annual precipitation here is around 600–650 mm, with the highest precipitation recorded in the summer months of June–August.

During the investigated period, the weather in the study area was typical for summer in southern Poland. In this time, there were several rainy events in the Opole Voivodeship, but the total rainfall was slightly below the long-term average. Low-pressure weather associated with precipitation occurred several times. On July 24, the region was affected by an atmospheric front, but there were no intense rainfalls. On July 26–27, there was a cut-off low here, which caused passing showers and local thunderstorms. On July 30–31, the Frieda low-pressure system prevailed in the region, and there were locally intense rainfalls and thunderstorms. In August, high rainfall was recorded in the region, sometimes accompanied by thunderstorms, but of local extent. Thus, on August 6–7, a cut-off low with a cold front was located here, and there were locally heavy rainfalls. From August 11, the region was under a low-pressure system, with relatively frequent local thunderstorms associated with intense rainfall.

2.2 | CML data

Acquisition of rain rate values from CML data requires detailed signal processing between two antennas. Typically, the transmitted signal level (TSL) and received signal level (RSL) can be used for this purpose. The difference between them, called transmitted minus received signal level (TRSL), represents a total signal path loss which includes not only loses caused by rainfall, but also gaseous attenuation, free-space loss and antenna gains (Fencl et al., 2021). The TRSL fluctuations caused by weather and artificial factors (van Leth et al., 2018) are visible on various time scales, including clear sky conditions (Chwala & Kunstmann, 2019). Therefore, a classification should be carried out with the aim of separating the rain-inducted episodes from the dry ones. Two main approaches can be used for this task. The first one relies on the temporal comparison of fluctuations of CML data at a given link with other links in close vicinity (Overeem et al., 2016a, 2016b). The second focuses on the analysis of each CML link separately, using, e.g., specific

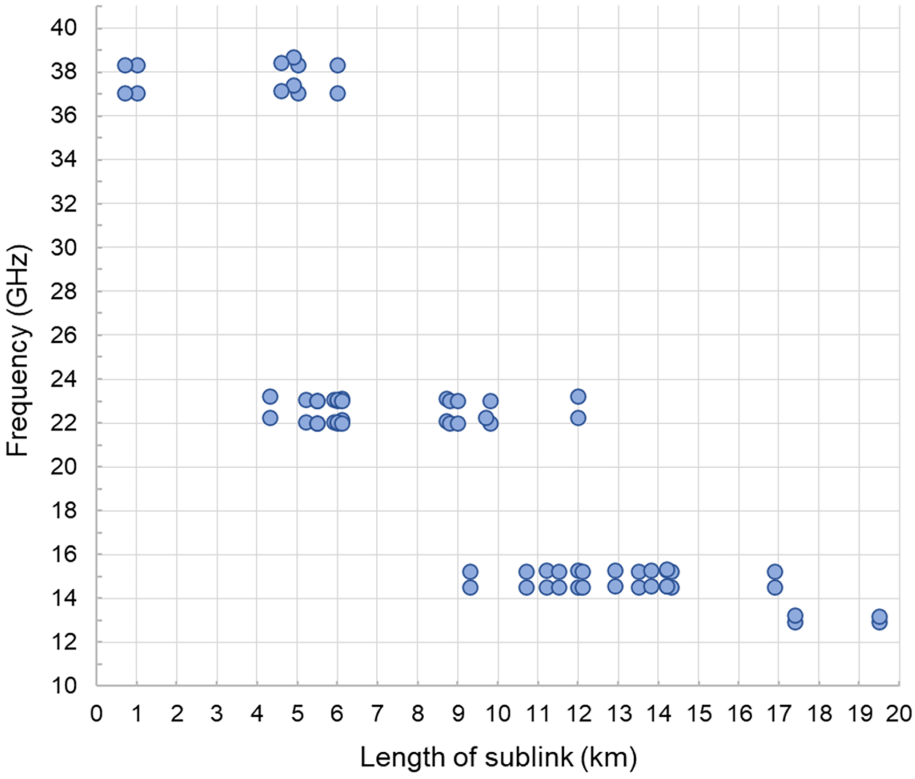

FIGURE 2 The relationship between the frequencies and lengths of the sublinks shown in Figure 1.

threshold to sliding-window standard deviations of TRSL time series, Fourier transform power spectra of a sliding window, Markov switching models and geostationary satellites or is based on classification features (Cherkassky et al., 2014; Chwala et al., 2012; Schleiss & Berne, 2010; van het Schip et al., 2017; Wang et al., 2012).

After detecting rain events in TRSL time series, the baseline of the dry period has to be determined. In the next step, by subtracting this baseline attenuation from the actual attenuation recorded during the rainy period (TRSL classified as wet), rain-inducted attenuation can be calculated. A rain-inducted attenuation delivered in such a way still needs to be corrected due to the wet antenna (Blevis, 1965), which is dependent on rainfall intensity and may cause additional attenuation up to 9 dB (Fencl et al., 2019). Therefore, wet antenna attenuation (WAA) is one of the crucial elements in CML signal pre-processing. This rain-induced and WAA-corrected attenuation A (dB) can then be converted to the rain rates (CML) using the relation:

$$A = a \cdot CML^{b} \cdot L \tag{1}$$

where CML is a rain rate (mm h^{-1}), L is the distance between transmitter and receiver (km), while a and b are coefficients dependent on the frequency, polarization, raindrop temperature and, in a smaller part, on the drop size distribution (Berne & Uijlenhoet, 2007).

The CML network topology is in the form of strips of different lengths located at different places (Figure 1). In this study, we used 67 microwave links in Opole Voivodeship obtained from the commercial company NetWorkS! (https://www.networks.pl/), which operates telecommunications networks. The TSL and RSL were stored with a 15-min interval and frequency range between approx. 7.5 and 85.0 GHz with a length ranging from 0.4 to 26.1 km. For our analyses, we have selected only those sublinks that have frequencies up to 40 GHz, to avoid strong signals dependency to the drop size distribution. The attenuation A is determined in each 15-min period as the difference between the maximum TSL value and the minimum RSL value in that period (Ostrometzky & Eshel, 2018). Figure 2 shows the relationship between the frequencies of the individual sublinks and their lengths, which illustrates the use of lower frequencies for longer sublinks. This is because, in order to prevent complete signal loss for longer links, it is necessary to use frequencies at which rain-induced specific attenuation is lower, which ensured at lower frequencies (Overeem et al., 2016a).

Each sublink was processed separately. For dry-wet classification, we adopted the spectral time-series analysis method based on the short-time Fourier transform, described by Chwala et al. (2012). In such an approach,

the wet period spectra show a significant discrepancy to the mean dry spectra. A threshold used for the classification of spectral amplitudes sums and spectrum division frequency was optimally determined based on data from rain gauges. For wet antenna correction, we used a time-dependent model developed by Schleiss et al. (2013) with values of parameters proposed in the paper. Finally, the rain rates were estimated using Equation 1, where a and b coefficients were derived from International Telecommunication Union – Radiocommunication Sector (ITU-R) recommendation (ITU-R, 2005).

2.3 | Rain gauge data

The Polish national meteorological and hydrological service (NMHS), provided by the Institute of Meteorology and Water Management – National Research Institute (IMGW), operates a nationwide rain gauge manual and telemetric networks.

As regards manual rain gauges, the measurement network uses Hellmann-type devices. Manual rain gauges are highly reliable, but their data are unavailable in real-time. The measurements are performed once a day (at 06:00 UTC). The network of such devices counts 23 stations in the area of interest (Figure 1b).

The network of telemetric rain gauges provides operationally 10-min rainfall totals G from approximately 500 precipitation stations. Most of them, however, are devices of tipping-bucket design characterised by high unreliability (Hoffmann et al., 2016; Segovia-Cardozo et al., 2021). Each precipitation station is equipped with two sensors: heated and unheated. The heated ones are year-round as they allow the measurement of the water content of snowfall, while the unheated ones operate in the warm part of the year, which in Poland lasts from April to October.

Quality control of telemetric precipitation data at IMGW is carried out with the dedicated automatic RainGaugeQC system in real time (Ośródka et al., 2022). The data are then spatially interpolated using the ordinary Kriging method to obtain the precipitation field G_{int}.

2.4 | Weather radar data

The Polish weather radar network POLRAD, which is operated by IMGW, is currently undergoing modernisation. Finally, it will consist of 10 Doppler radars with a dual-polarised radar beam, manufactured by Leonardo Germany. Data from the POLRAD network are operationally supplemented by radar data from several neighbouring countries. Opole Voivodeship (province) is covered by observations from three Polish and one Czech radars.

Raw radar reflectivity data are generated as 3D files in polar coordinates. The data after quality control performed with the external RADVOL-QC system (Ośródka et al., 2014; Ośródka & Szturc, 2022) are processed by the Rainbow 5 radar system into final 2D radar products. Precipitation products are generated every 10 min by the Rainbow 5 system using the surface rainfall intensity (SRI) algorithm and then processed into 10-min totals using the precipitation accumulation (PAC) algorithm. At the same time, quality fields are generated based on analyses of particular errors disturbing radar data. Then the rainfall data from the individual radars are merged into composite maps R using the quality of the individual data as a criterion (Jurczyk, Szturc, & Ośródka, 2020).

The final stage of radar rainfall processing is the adjustment to telemetric rain gauge data, which is carried out in two steps: first, the mean field bias method is applied to each radar; in the second step, the radar composite data are locally adjusted using interpolated G/R ratio values (Jurczyk, Szturc, Otop, et al., 2020). As a result, a radar field R_{cor} is generated.

2.5 | Meteorological satellite data

The satellite precipitation products used in IMGW are generated based on visible and infrared channels from EUMETSAT Meteosat series. Although precipitation intensity is not estimated directly from these data, software provided within the EUMETSAT NWC-SAF programme (http://www.nwcsaf.org/) enables the generation of precipitation products based on the physical properties of clouds. The products used for this purpose are Convective Rainfall Rate from Cloud – Physical Properties, Precipitating Clouds from Cloud – Physical Properties, Convective Rainfall Rate from Cloud and Precipitating Clouds from Cloud. Employing these products and an algorithm developed at IMGW (Jurczyk, Szturc, Otop, et al., 2020), 10-min precipitation accumulations are generated with a spatial resolution taken from the resolution of the raw Meteosat data, approximately 5 km × 6 km for the area of Poland.

2.6 | RainGRS multi-source precipitation estimates

Multi-source precipitation field estimates (QPEs) are produced every 10 min by the RainGRS system, which combines rain gauge, radar and satellite precipitation data

(Jurczyk, Szturc, Otop, et al., 2020) with a high spatial resolution of 1 km × 1 km.

It is widely considered that radar rainfall best represents the spatial distribution of the rainfall field, while a network of rain gauges effectively reduces the bias of this estimation. Satellite rainfall, in turn, plays a role mainly as a supplement during deficiencies in the other data. An essential feature of this system is the use of quantitative information about the spatial distribution of the quality of the individual input data, attributed to them when quality checks are performed. The algorithm for combining these data is based on conditional merging, which attempts to enhance individual input data's strengths and reduce their weaknesses' impact (Jurczyk, Szturc, Otop, et al., 2020). Precipitation estimates (*GRS*) are completed with fields of quality index (*QI*), which is generated as unitless quantity from 0 to 1 ("1" for data of perfect quality).

It should be noted that input to RainGRS, i.e., data from telemetric rain gauges, weather radar and satellite, typically significantly underestimate rainfall compared with data from manual rain gauges (Urban & Strug, 2021).

Apart from operationally generated RainGRS fields, their reanalyses are also employed in this paper. They are generated as daily accumulations with a delay based on more complete input data than in real time. Moreover, the fields are adjusted employing data from manual rain gauges. The latter are a crucial input to the reanalysis system due to their accuracy, even though they are point measurements, less frequently available and with a long delay.

3 | METHODOLOGY FOR GENERATING CML-BASED PRECIPITATION FIELD

3.1 | Quality control of precipitation data from CMLs using multi-source estimates

Quality control of precipitation data obtained from CML data is performed for each sublink separately, based on multi-source precipitation estimates (QPEs) provided by the RainGRS system. As the RainGRS and CML-based estimates have different temporal resolutions of 10 and 15 min, respectively, the half-hourly accumulations were employed as a common time interval. For each link, the precipitation accumulation is determined from *GRS* values in pixels along the entire link (see Figure 1), considering grids of 3 pixels × 3 pixels. For each grid a mean precipitation value and mean of quality index are calculated. If at least half of the grids have the mean quality above the preset threshold 0.85 (which is related to high reliability of the estimate), then the mean precipitation value for the entire link is calculated from all grids ($\overline{GRS_{CML}}$); otherwise, the link is processed without quality control.

For each sublink, the CML-based 30-min precipitation value (CML) changes to "no data" if it showed no or relatively low precipitation and $\overline{GRS_{CML}}$ indicated significant precipitation, or in reverse case:

$$\begin{aligned} &\text{If } \left((CML < 0.3 \text{ mm}) \text{ and } \left(\overline{GRS_{CML}} > 1.0 \text{ mm}\right)\right) \\ &\text{or } \left((CML > 1.0 \text{ mm}) \text{ and } \left(\overline{GRS_{CML}} > 0.3 \text{ mm}\right)\right), \\ &\text{then } CML = \text{"no data} \end{aligned} \tag{2}$$

or if the CML indicated a very high precipitation that is not confirmed by $\overline{GRS_{CML}}$:

$$\begin{aligned} &\text{if } \left(CML > 80 \text{ mm}\right) \text{ and } \left(CML > 3.0\ \overline{GRS_{CML}}\right) \\ &\text{then } CML = \text{"no data"} \end{aligned} \tag{3}$$

Otherwise, precipitation values in individual sublinks are left unchanged. All the above threshold values and parameters were determined empirically by manual tuning based on analyses of CML-derived precipitation outliers.

3.2 | Estimation of point precipitation from CMLs data

Generally, each link consists of more than one sublink (frequency), and mostly each sublink determines a different precipitation value estimated from the signal attenuation. Thus, one precipitation value has to be determined from all sublinks available in a link.

Two versions of precipitation determination from all available sublinks were analysed:

- Mean-1: Mean of precipitation from all sublinks.
- Mean-2: A slightly more advanced algorithm is based on decision tree taking into account the division of the sublinks into two classes: with and without precipitation, then counting the mean only in the more numerous class, while the data from the other class are ignored. If the sizes of these classes are equal, then the mean of all data is counted, as in the first version.

The value of precipitation determined by both these methods is a path-integrated value, referring to the precipitation along the entire link. Thus, for each link the precipitation value should be assigned to a specific point

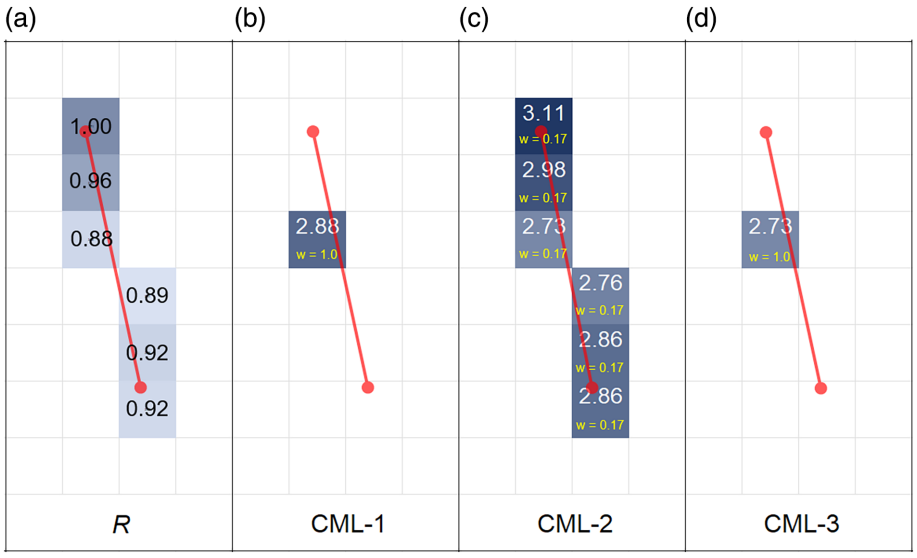

FIGURE 3 Example of (a) radar-based precipitation field, and assigning precipitation values to individual CML obtained by methods: (b) CML-1, (c) CML-2 and (d) CML-3. The smaller yellow font indicates the weight values (w) of the individual virtual rain gauges. Link located near the town of Opole is marked by a red line. Half-hourly accumulation from 30 July 2022, 10:30 UTC.

or set of pixels, here called virtual rain gauges. This is particularly important when having data from longer links and in the case of a more spatially variable precipitation field.

The following three ways of assigning appropriate precipitation values to individual links are proposed:

- CML-1: The mean CML-based precipitation along the entire link is assigned to the pixel at its centre (hereinafter referred to as $CML-1$). Its weight for spatial interpolation is set to 1.0.
- CML-2: The CML-based precipitation is distributed along the entire link based on the distribution of radar precipitation along this link (hereinafter referred to as $CML-2$). Thus, linear sequence of virtual rain gauges is created, spaced every pixel (here every 1 km) along this CML. Each virtual rain gauge is given a precipitation value and weight of:

$$CML-2_i = CML \cdot \frac{R_i}{\sum_{i=1}^{N_{CML}} R_i},\ w = \frac{1}{N_{CML}} \tag{4}$$

where i is a number of virtual rain gauge; R_i is the radar precipitation in pixel related to i-th virtual rain gauge; N_{CML} is the number of the virtual rain gauges. The total weight of all virtual rain gauges along a given link is always 1.0.

- CML-3: The CML-based precipitation is also distributed along the entire link based on the radar precipitation distribution, but the precipitation from only one virtual rain gauge located at the pixel in the centre of the link is taken for interpolation (hereinafter referred to as $CML-3$). It is assigned a weight of $w = 1.0$.

The spatial distribution of the precipitation field in the CML-2 and CML-3 versions is taken directly from the weather radar data instead of from RainGRS estimates. This results from the fact that merging the radar data with other precipitation estimates, especially from rain gauges, improves the precipitation values at individual pixels but may distort its spatial distribution, which is less consistent in the multi-source field. Figure 3 illustrates results of above methods of assigning precipitation values to individual CML, applying virtual rain gauges for a short (6-km long) link located near the town of Opole (see Figure 1b).

The precipitation in virtual rain gauges, determined by means of the methods mentioned above, is then spatially interpolated (Section 3.3).

3.3 | Generating CML-based precipitation field

The next step in this work is spatial interpolation of values from virtual rain gauges which were introduced in Section 3.1. Spatial interpolation of the CML-derived precipitation data (CML_{int}) was carried out using the inverse distance method (IDW), in which the weights depend not only on the distance from individual rain gauges but also on their weights. This technique can be written with the following formula:

$$CML_{int}(x,y) = \frac{\sum_{i=1}^{n}\left(\frac{CML_i \cdot w_i}{d_i^2}\right)}{\sum_{i=1}^{n}\left(\frac{w_i}{d_i^2}\right)} \tag{5}$$

where x, y are the coordinates of the given pixel; $i = 1,\ldots,n$; n is the number of virtual rain gauges related

to CMLs; d_i is the distance from the pixel (x, y) to the $i-$th virtual rain gauge; w_i is the weight of the $i-$th virtual rain gauge. The most important parameters of the algorithm are the radius of influence of the rain gauges and the number of gauges taken for interpolation, which are set to 75 km and 10, respectively. For the CML-2 version, different parameters were chosen because of a much higher number of virtual gauges: 35 km for a radius of influence and no limit for the number of gauges.

4 | VERIFICATION OF CML-BASED PRECIPITATION FIELD

4.1 | Methodology of verification

The main objective of this work is to assess the reliability of the precipitation information extracted from signal attenuation data in microwave links. It is essential to have some reference to verify precipitation data calculated based on attenuation in CMLs. In the case of precipitation, which is highly temporally and spatially variable and therefore difficult to measure and estimate, it is always a problem to choose the most appropriate reference. In the present work, it was decided to apply two references:

- Point measurements from the network of manual rain gauges,
- Multi-source precipitation field estimates from RainGRS operational and after reanalysis.

Measurements with manual rain gauges are considered the most accurate, as they are direct measurements made with a simple but reliable instrument. However, due to their point-based nature, direct comparisons are only possible for their locations, which are not very numerous. It limits the possibility of very accurate verification, especially in the case of point data requiring spatial interpolation to obtain values at locations of reference gauges, which introduces errors.

In contrast, RainGRS estimates are generated as fields with high 1-km spatial resolution, which makes verification easier. However, their reliability, which is high in comparison with individual measurement techniques separately, is nevertheless strongly dependent on their local uncertainties. Typically, input data to RainGRS underestimate precipitation values, which consequently transforms directly into the model estimates. So, for daily verification purposes, we used the version of the RainGRS system called RainGRS Clim which generates estimates after reanalysis, i.e., after adjusting the *GRS* values using observations derived from relatively dense network of the manual rain gauges (Jurczyk et al., 2023). Thanks to the adjustment the RainGRS Clim estimates are nearly unbiased and can be considered as a reliable reference for daily precipitation accumulations.

Since manual rain gauges are only available with a daily temporal resolution so for half-hourly verification the operational RainGRS data can be employed.

The CML-based precipitation data were verified both before and after applying the QC algorithm described in Section 3.1. The verification was conducted on daily and half-hourly accumulations from July 19 to August 18, 2022. Data from days without precipitation have been excluded from this period.

The statistics BIAS, MAE, RMSE, RRSE and correlation coefficient CC were counted against reference observations:

- Statistical bias:

$$BIAS = \frac{1}{n}\sum_{i=1}^{n}(E_i - O_i) \tag{6}$$

- Root mean square error:

$$RMSE = \left(\frac{1}{n}\sum_{i=1}^{n}(E_i - O_i)^2\right)^{0.5} \tag{7}$$

- Root relative square error:

$$RRSE = \left(\frac{\sum_{i=1}^{n}(E_i - O_i)^2}{\sum_{i=1}^{n}(O_i - \overline{O})^2}\right)^{0.5} \tag{8}$$

- Pearson correlation coefficient:

$$CC = \frac{\sum_{i=1}^{n}(E_i - \overline{E})(O_i - \overline{O})}{\left(\sum_{i=1}^{n}(O_i - \overline{O})^2 \sum_{i=1}^{n}(E_i - \overline{E})^2\right)^{0.5}}, \tag{9}$$

where E_i is the estimate of the evaluated quantity; O_i is the reference observation; i is the reference gauge or pixel number of the computational domain; n is the number of reference gauges or pixels in the domain $\overline{E}$ and $\overline{O}$ are the mean values.

TABLE 1 Statistics for precipitation values determined for CMLs before and after quality control applying Mean-1 and Mean-2 methods, using half-hourly RainGRS accumulations (in mm) as a reference, July 19 – August 18, 2022.

Estimate	BIAS (mm)	RMSE (mm)	RRSE (−)	CC (−)
Before quality control				
Mean-1	−0.02	0.62	0.93	0.71
Mean-2	−0.02	0.63	0.94	0.69
After quality control				
Mean-1	−0.01	0.67	1.00	0.82
Mean-2	−0.02	0.68	1.00	0.82

4.2 | Verification of method for precipitation determination from available sublinks

The effectiveness of the two proposed methods of precipitation determination from available sublinks, Mean-1 and Mean-2 was tested on 30-min RainGRS accumulations. The precipitation values estimated for a given link were compared with the precipitation values estimated by RainGRS as the integrated precipitation from all pixels along the link. Precipitation at each 1 km × 1 km pixel located within a given link was determined as the average of a 3 pixels × 3 pixels grid. Statistics for CML-based precipitation determined using methods described in Section 3.2 are presented in Table 1.

The differences between the results for the both versions are minor considering all the statistics counted (e.g., for RMSE they are at most one hundredth of a mm), so it can be assumed that they perform comparably. Consequently, it can be concluded that the exclusion of certain sublinks from the precipitation estimation, based on a comparison of the counts of sublinks that indicate whether the precipitation occurs or not, does not improve the results. However, the use of the Mean-2 algorithm can prevent obvious errors in precipitation estimation in case of erroneous precipitation values obtained for certain sublinks, so it was decided to use the Mean-2 method in this study.

Higher correlation coefficient CC after quality control indicates that the spatial distribution of the rainfall field has clearly improved. On the other hand, higher values of metrics using deviations from reference values were recorded. Bearing in mind the general underestimation of CML-based rainfall, it can be concluded that QC eliminated sublinks indicating high rainfall values, which resulted in a deterioration of metrics based on differences in values.

4.3 | Verification of daily precipitation accumulations

A spatial analysis of the reliability of CML-based precipitation estimates was carried out on spatially interpolated CML fields, considering the different methods of generating virtual rain gauges: CML-1, CML-2 and CML-3. These fields were compared with point rain gauge measurements only at their locations and with RainGRS estimates for the whole precipitation fields. Table 2 summarises the statistics of CML-based precipitation, calculated before and after quality control using data from the manual rain gauges as a reference at their locations.

Regarding the various methods of assigning precipitation values to a given link, namely versions CML-1, 2 and 3, there are also no significant differences in the statistics. The CML-2 version, i.e. precipitation estimate $CML-2_{int}$, which involves using the spatial distribution of the radar precipitation field to estimate the precipitation distribution along a given link, is considered as optimal.

The quality control improved the reliability of the CML-based estimates, which is reflected in most the counted statistics. Taking the CML-2 method, RMSE is unchanged, while CC values increased from 0.818 to 0.854. After QC, the values of the individual statistics are closer to those calculated for other precipitation field estimates, such as interpolated telemetric rain gauges, weather radars and multi-source estimates, but the differences are still noticeable. In comparison with the satellite precipitation field, CML-based precipitation is significantly better. Figure 4 shows graphs illustrating the results presented in Table 2 for all versions of assigning precipitation values to individual links.

Results of the spatial analysis on all 1 km × 1 km pixels located within the Opole Voivodeship are presented in Table 3, with values of the individual statistics analogously to Table 2. This analysis was carried out on RainGRS reanalyses, that is, multi-source estimates of the precipitation field adjusted to data from manual rain gauges.

The results presented in Table 3 for the three methods of assigning appropriate precipitation values to individual links, that is, CML-1, 2 and 3, indicate that the $CML-2_{int}$ estimates are closest to the reference data, which are the RainGRS precipitation field reanalyses. This is consistent with the verification result on the point

Estimate	BIAS (mm)	RMSE (mm)	RRSE (–)	CC (–)
Before quality control				
$CML-1_{int}$	−1.00	4.31	0.70	0.825
$CML-2_{int}$	−1.06	4.37	0.70	0.818
$CML-3_{int}$	−1.02	4.31	0.70	0.817
After quality control				
$CML-1_{int}$	−1.20	4.39	0.71	0.847
$CML-2_{int}$	−1.27	4.37	0.71	0.854
$CML-3_{int}$	−1.18	4.35	0.70	0.840
Other estimates				
G_{int}	−0.92	2.91	0.48	0.905
R_{cor}	−0.05	2.14	0.35	0.938
S	−1.77	6.02	0.96	0.486
GRS	−0.35	2.04	0.34	0.952

TABLE 2 Results of verification of CML-based precipitation before and after quality control, as well as interpolated telemetric rain gauges (G_{int}), corrected radar (R_{cor}), satellite (S) and operational RainGRS (GRS) data, using manual rain gauge data as a reference, daily accumulations (in mm) from July 19 – August 18, 2022.

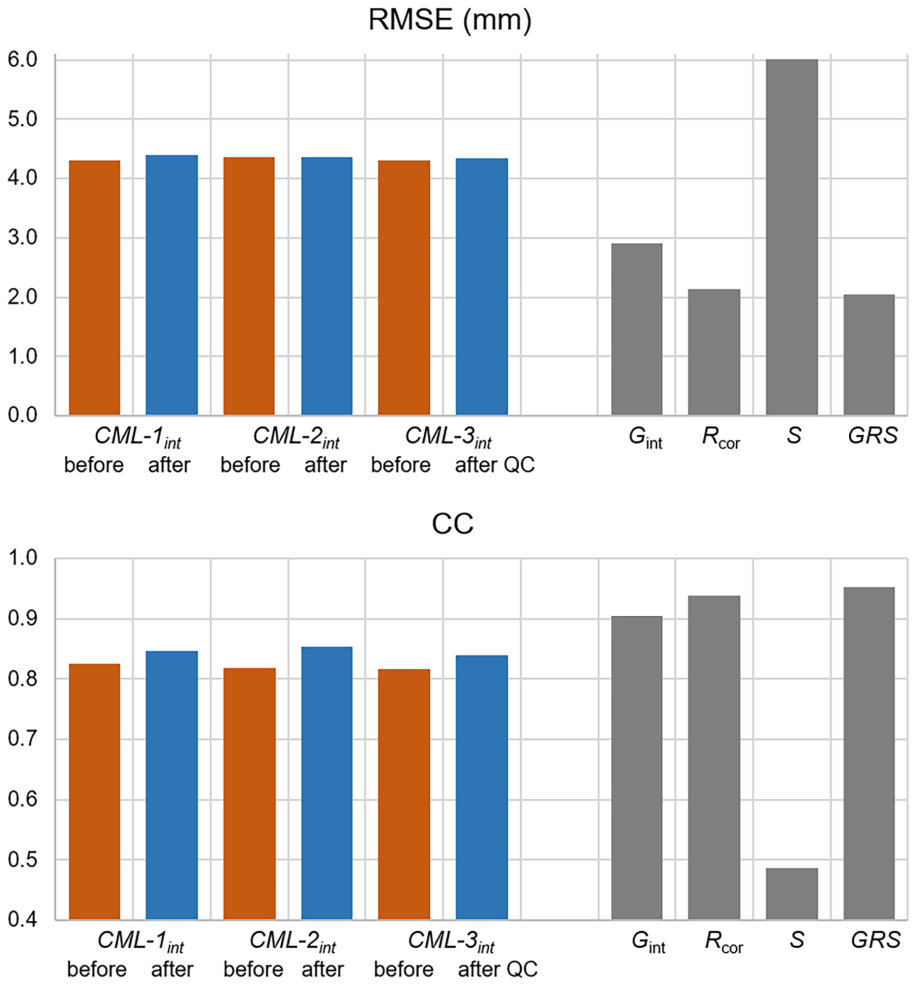

FIGURE 4 RMSE (upper) and correlation coefficient CC (bottom) of CML-based precipitation ($CML-1_{int}, CML-2_{int}, and\ CML-3_{int}$) determined before (in brown) and after (in blue) quality control as well as telemetric rain gauges (G_{int}), corrected radar (R_{cor}), satellite (S) and operational RainGRS (GRS) data (in grey). Manual rain gauge data as a reference. Daily accumulations from July 19 – August 18, 2022.

data presented in Table 2; however, the improvement is more evident in this spatial verification. It can be explained by the fact that the CML-2 version (spatially distributed precipitation along each link) shows its advantages when the spatial distributions of the precipitation field are compared. Therefore, the choice of the method of precipitation field generation based on attenuation measurements in the CML depends on the specific

TABLE 3 Results of verification of CML-based precipitation before and after quality control, as well as interpolated telemetric rain gauges (G_{int}), corrected radar (R_{cor}) and satellite (S), using RainGRS reanalyses as a reference, daily accumulations (in mm) from July 19 – August 18, 2022.

Estimate	BIAS (mm)	RMSE (mm)	RRSE (–)	CC (–)
Before quality control				
$CML-1_{int}$	−1.27	3.78	1.10	0.458
$CML-2_{int}$	−1.36	3.74	1.07	0.474
$CML-3_{int}$	−1.27	3.82	1.11	0.454
After quality control				
$CML-1_{int}$	−1.62	3.75	1.05	0.507
$CML-2_{int}$	−1.68	3.72	1.03	0.527
$CML-3_{int}$	−1.59	3.75	1.05	0.505
Other estimates				
G_{int}	−1.12	2.88	0.84	0.604
R_{cor}	−0.18	1.37	0.40	0.950
S	−1.88	4.56	1.29	0.373

application of the obtained precipitation data, especially since the differences between the verification results of the different methods are insignificant.

Similarly to verification with manual rain gauges (Table 2), results after QC also improved, for example for $CML-2_{int}$ the CC increased from 0.474 to 0.527, and RMSE decreased from 3.74 to 3.72 mm. Comparison of metrics computed for CML-based data with statistics for other precipitation estimates shows that the CML-based precipitation fields are distinctly worse than radar-based estimates but only slightly worse than spatially interpolated telemetric rain gauge data. At the same time, they are significantly better than satellite-based estimates.

4.4 | Verification of half-hourly precipitation accumulations

From the point of view of the potential operational use of CML-based precipitation data, it is crucial to evaluate the reliability of the data with a temporal resolution much higher than daily. As the RainGRS and CML-based estimates have different temporal resolutions of 10 and 15 min, respectively, the half-hourly accumulations were employed, using operational RainGRS data as a reference (see Section 3.1).

The results of verification on the half-hourly data, presented in Table 4 and Figure 5, confirm findings for the daily data analysis in terms of assigning appropriate precipitation values to individual links. The CML-2 method slightly outperforms the others, although there are no significant differences between the reliabilities of precipitation estimates produced by all the techniques. The quality control slightly reduced errors in CML-derived estimates: RMSE decreased from 0.32 to 0.31 mm, whereas CC improved from 0.761 to 0.820 for the best CML-2 method (Table 4).

Regarding the RMSE, CML-based precipitation for the CML-2 method after QC has higher reliability than satellite-based estimates and similar to interpolated rain gauge estimates (0.31 vs. 0.41 and 0.29 mm, respectively). Concerning the correlation coefficient, however, it has higher reliability compared with rain gauges (0.820 vs. 0.669) and significantly higher compared with satellite estimates (0.820 vs. 0.296) (Table 4).

It is important to note that operational RainGRS data can be subject to errors. Therefore, when using operational RainGRS as a reference for sub-hourly verification, a substantial portion of the uncertainty in assessed estimates (expressed by BIAS, RMSE and RRSE) may be associated with these errors. Nevertheless, operational RainGRS remains the best available reference for this temporal resolution.

5 | ANALYSIS OF THE RESULTS

5.1 | Influence of link characteristics on reliability of precipitation estimates

An analysis of the influence of the CMLs characteristics such as length and frequency on quality of precipitation estimates obtained with CML-2 method (see Section 3.2) was carried out. The reliability of these estimates was determined by root relative square error (RRSE), using RainGRS estimates as reference. Calculations were performed on half-hourly values for individual days and links.

Figure 6a shows a graph illustrating the magnitude of relative precipitation estimation errors (RRSE) as a

Estimate	BIAS (mm)	RMSE (mm)	RRSE (–)	CC (–)
Before quality control				
$CML-1_{int}$	−0.01	0.35	0.87	0.724
$CML-2_{int}$	−0.01	0.32	0.80	0.761
$CML-3_{int}$	−0.01	0.34	0.85	0.743
After quality control				
$CML-1_{int}$	−0.02	0.34	0.84	0.791
$CML-2_{int}$	−0.02	0.31	0.76	0.820
$CML-3_{int}$	−0.02	0.33	0.81	0.815
Other estimates				
G_{int}	−0.01	0.29	0.76	0.669
R_{cor}	0.00	0.06	0.15	0.988
S	−0.03	0.41	1.08	0.296

TABLE 4 Results of verification of CML-based precipitation before and after quality control, as well as interpolated telemetric rain gauges (G_{int}), corrected radar (R_{cor}) and satellite (S) data, using RainGRS data as a reference, half-hourly accumulations (in mm) from July 19 – August 18, 2022.

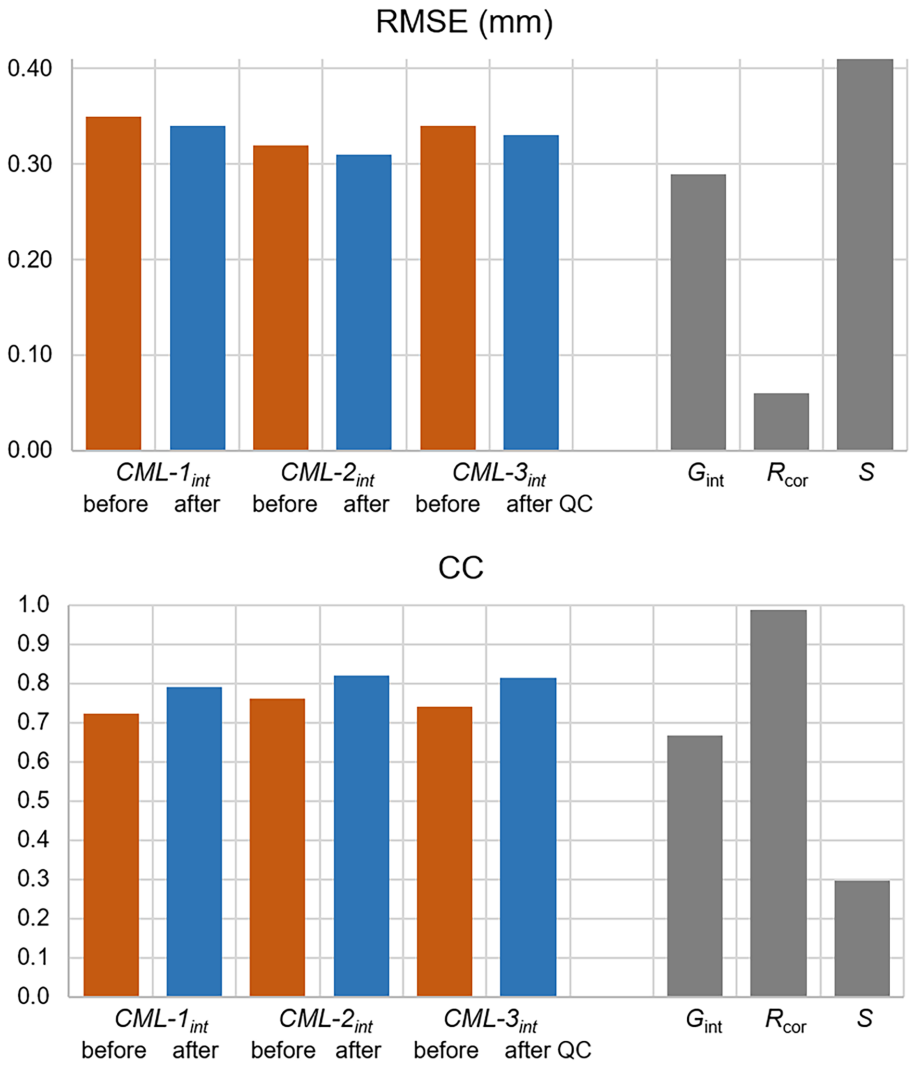

FIGURE 5 RMSE and correlation coefficient CC of CML-based precipitation ($CML-1_{int}, CML-2_{int}, and\ CML-3_{int}$) determined before (in brown) and after (in blue) quality control as well as telemetric rain gauges (G_{int}), corrected radar (R_{cor}) and satellite (S) data (in grey). RainGRS as a reference. Half-hourly accumulations from July 19 – August 18, 2022.

function of link length L. It can be noted that larger errors are associated with the shortest links up to 1 km in length. There are no links of length above 1 km and below 4 km in the analysed area, so it is impossible to say what is the limiting length below which the reliability of the precipitation estimate is significantly lower. The

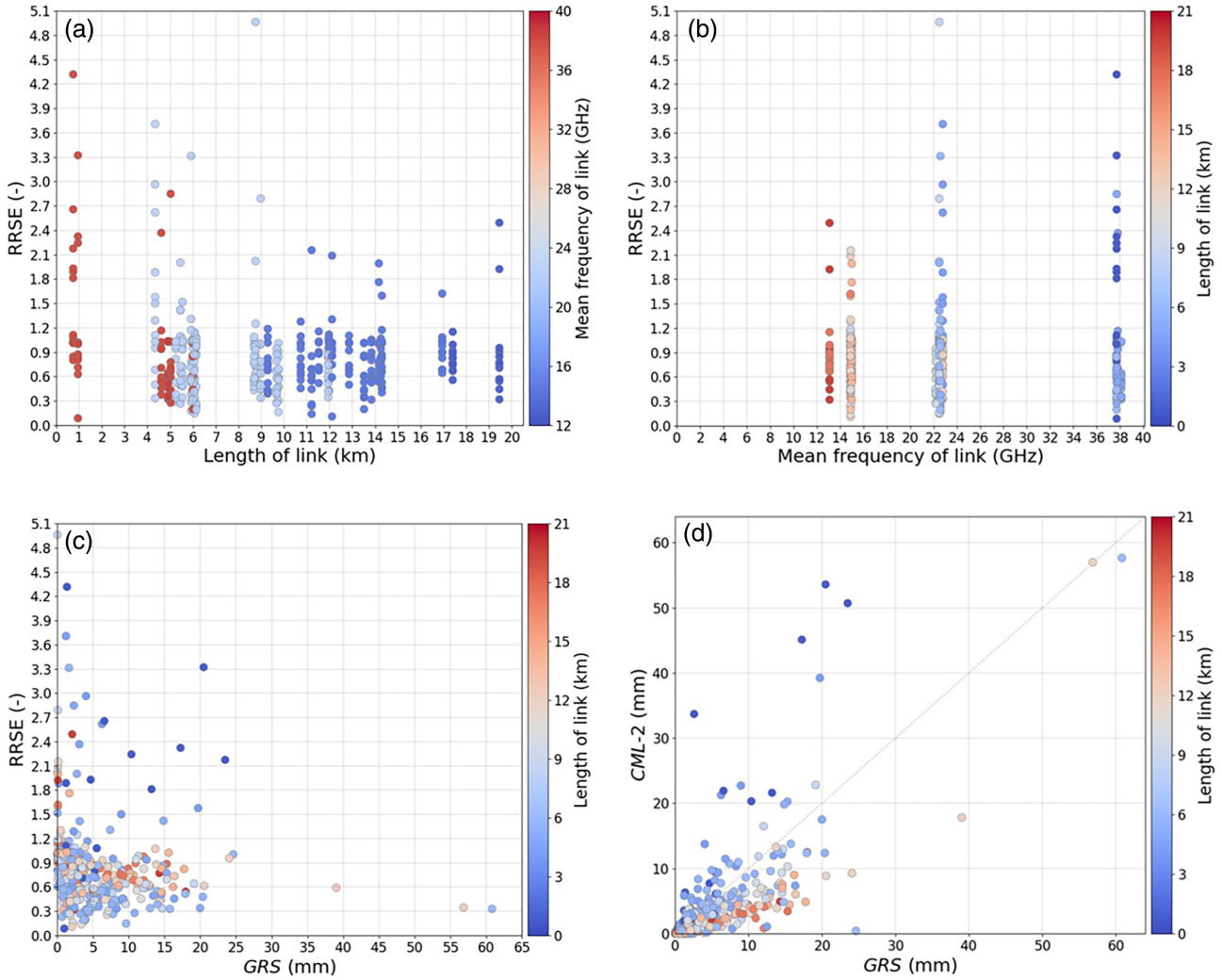

FIGURE 6 Relationships between the relative error of precipitation estimation RRSE and: (a) link length, (b) frequency and (c) daily precipitation accumulation, as well as: (d) relationship of the precipitation estimated by the CML-2 method and the *GRS* reference value.

limited size of the available data set does not enable to draw general conclusions; however, this observation is confirmed in literature (Chwala & Kunstmann, 2019; Fencl et al., 2019). It is reported that raindrops on the CML antennas lead to additional attenuation, resulting in an overestimation of rainfall especially in short links, as for shorter CMLs both antennas are more likely to get wet. The effect of wet antenna attenuation (WAA) is one of the dominant sources of error and was deeply analysed for very short links by Fencl et al. (2019). They notice systematic behaviour indicating that WAA magnitude is dependent on rainfall intensity and substantially contributes to total CML attenuation, especially when considering shorter CMLs and clearly dominates over raindrop path attenuation during light precipitation rates, below $2\,\mathrm{mm\,h^{-1}}$. The clear dependence of bias on CML length is shown in Figure 6, especially in Figure 6d, where the largest biases are observed on short links which indicates the increased influence of WAA. For longer links the magnitude of the errors seems not to depend on the link length (Figure 6a).

Figure 6b shows the dependence of the RRSE on the average frequency used in a given link (the variation of individual sublink frequencies within a given link is small, as it is about 1 GHz). In this graph, high RRSE values significantly deviating from the average are associated with high signal frequencies, which are related with short links as can be seen from the clear correlation of link length with frequency shown in Figure 2. The relationship between RRSE and precipitation amount estimated by RainGRS (*GRS*) is depicted in Figure 6c. It can be clearly noticed that the largest errors occur at light precipitation on the shortest links (points in blue). In turn, Figure 6d presents the dependence between the precipitation estimated from attenuation in CMLs using the CML-2 method and the reference precipitation estimated

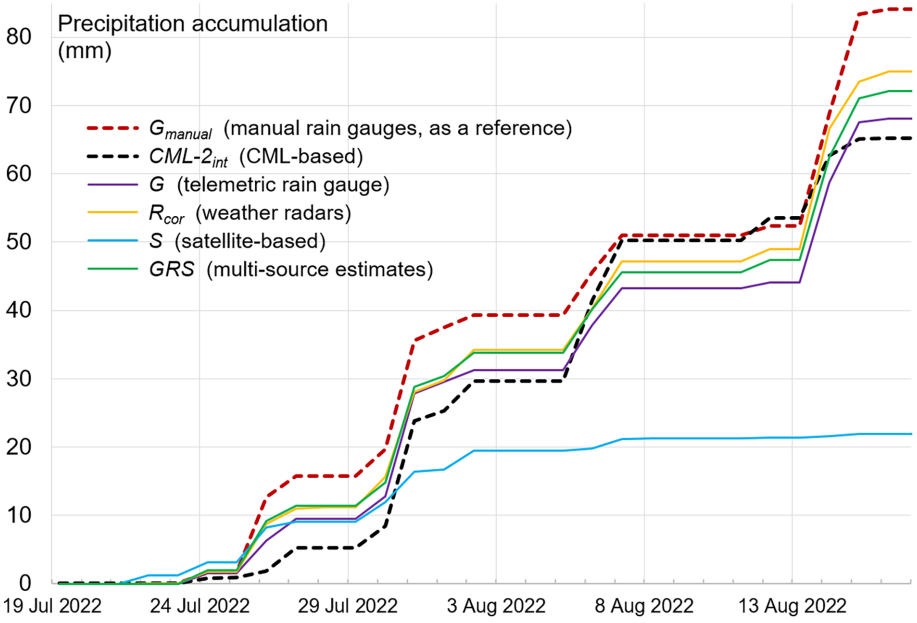

FIGURE 7 Cumulative daily precipitation accumulations (in mm) acquired from Opole manual rain gauge (G_{manual}), CML ($CML-2_{int}$) after quality control, telemetric rain gauge field (G_{int}), weather radars (R_{cor}), satellite (S) and multi-source RainGRS estimate (GRS). Dashed lines for CML-based precipitation and for manual rain gauges as a reference.

by the RainGRS system. Here, the erroneous values for short links observed in the previous graphs can be seen as well. However, it can also be noticed that the CML-based estimates are much more likely to be overestimated for shorter links (points in blue shades) and underestimated for longer links (red shades).

5.2 | Comparison of time-series estimates

Figure 7 shows cumulative daily precipitation accumulations for the location of the manual rain gauge station Opole, which is situated at one of the ends of a link that is about 6-km long, that is relatively short. For this location, the following cumulative daily accumulations are presented: from the manual rain gauge measurements as the reference, CML-based estimates obtained using the CML-2 method, and other estimates: from telemetric rain gauge network G_{int}, radar observations R_{cor}, satellite observations S and multi-source GRS for comparison.

The results shown in Figure 7 indicate correct detection of the precipitation occurrence using CML-based estimates with respect to measurements with manual rain gauge, while the estimation of the precipitation value is not satisfactory. However, no systematic error is observed, as the CML-based data estimates show over- or underestimation with differences of up to about 50% during the different events. Comparing the accumulations of CML-based precipitation with those of other estimates, it can be seen that CMLs produce estimates that are clearly superior to satellite-based ones, but worse than the others (from rain gauges, radars and GRS), especially when it comes to precipitation values, as the detection of precipitation occurrence is generally correct.

5.3 | Example of long-term rainfall accumulations

Figure 8 shows the long-term accumulations of precipitation fields that were generated from the CML data using the methodology proposed and described in this paper. These are: CML-based data before and after quality control (a, b), data used as reference: observations from manual rain gauges and reanalyses of the RainGRS estimates (c, d), as well as other estimates for comparison: data from interpolated telemetric gauges, weather radar estimate and satellite estimate (e, f, g). The precipitation fields were restricted here to the boundaries of Opole Voivodeship (see Figure 1).

The maps in Figure 8a–g show differences in the precipitation fields obtained by the various measurement and estimation techniques. This Figure clearly shows the impact of the data quality control procedure used, comparing Figure 8a,b with the references in Figure 8c,d. It can be noticed that the highest values of raw CML-based precipitation were significantly reduced after QC. Some of these inconsistencies between CML-based estimates and other precipitation field estimates are due to the fact that the CML network in the study area is not very dense (see Figure 1). For example, the intense precipitation at the northern border of the region recorded by the manual rain gauge, telemetric rain gauges and weather radars could not be seen by the CML because there is no link at this location. The same occurred in the south-eastern

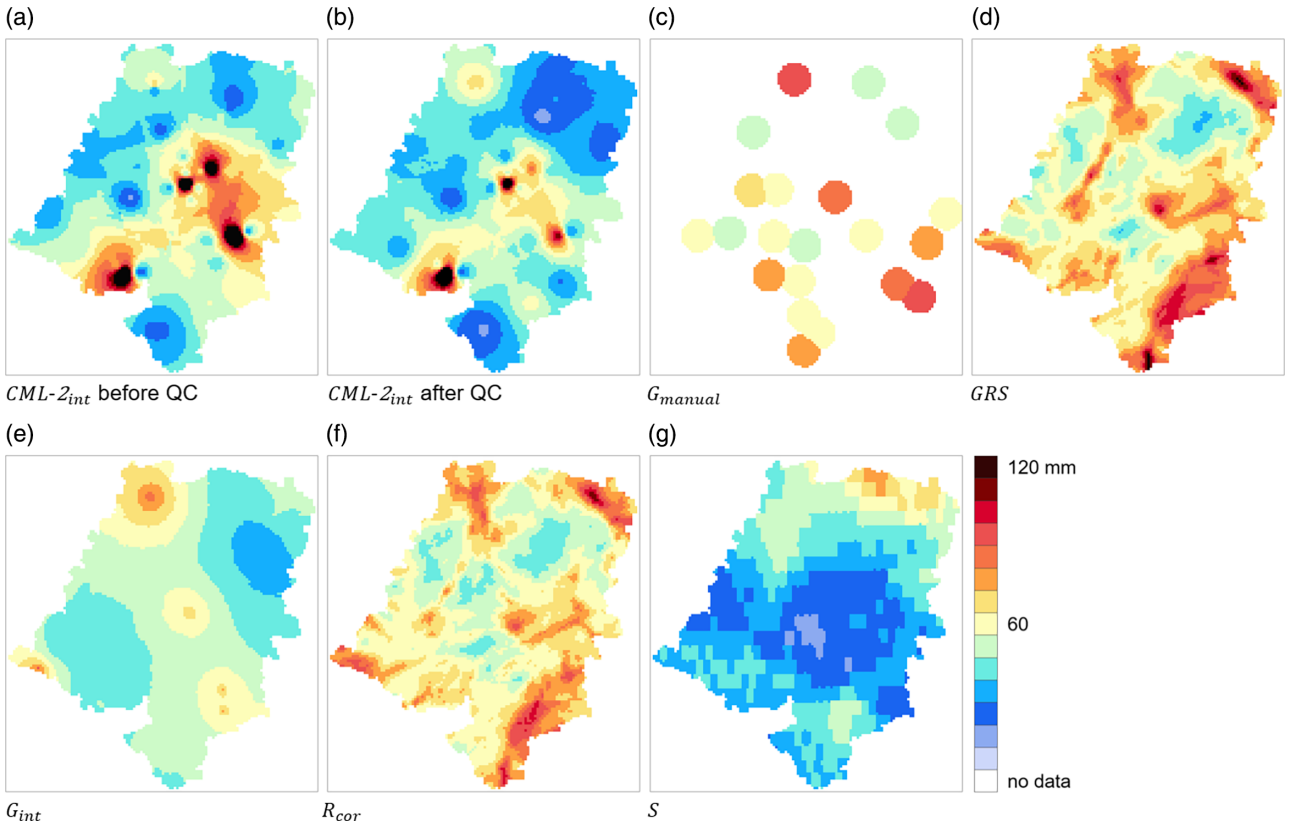

FIGURE 8 Long-term precipitation accumulations of CML-based precipitation $CML-2_{int}$ using CML-2 method: (a) before quality control and (b) after quality control; data used as reference: (c) observations from manual rain gauges G_{manual} and (d) reanalysis of the RainGRS estimate *GRS*, and other estimates: (e) interpolated data from telemetric gauges G_{int}, (f) weather radar estimate R_{cor} and (g) satellite estimate *S*. Accumulations from July 19 – August 18, 2022.

area along the region's border. It should be noted that the network of telemetric rain gauges is also not dense, resulting in rainfall that occurred in several places in the region not being detected by this network. However, they were detected by the radars, so that the *GRS* field takes them into account. The satellite field differs significantly from the others, which is also reflected in the results presented in this paper.

6 | CONCLUSIONS AND RECOMMENDATIONS FOR FURTHER WORK

This work aimed to evaluate the reliability of the precipitation estimation retrieved from attenuation in commercial microwave links (CML). Since a single link has several sublinks (frequencies), each of which may deliver various precipitation values, two different methods of precipitation determination described in Section 3.2 were tested. Then, in order to interpolate spatially these values, three different approaches were proposed in the same Section.

CML-based precipitation was verified by comparison with the point measurements from manual rain gauges and multi-source precipitation fields with high spatio-temporal resolution from RainGRS. By analysing the obtained result, the following can be concluded:

1. It is not clear which method of precipitation calculation from available sublinks is better. Thus, the analysis should be continued by applying more data from a larger area over a more extended period, considering different types of precipitation (seasons).
2. The CML-2 method, based on precipitation distribution along the link according to radar data and the creation of virtual rain gauges sequence depending on link length, slightly outperforms the others. Its advantages are noticeable in the analysis in which RainGRS estimates were used as a reference, and the spatial distributions of the precipitation field were compared.
3. The simple QC algorithms turned out not very effective as after the QC the reliability of CML-based precipitation estimates improved to a small extent. However, analyses of longer precipitation

accumulations showed that the highly overestimated values were significantly reduced as a result of QC.
4. Compared with other precipitation estimates, it was found that the CML-based precipitation fields are much worse than radar-derived estimates. At the same time, mostly they had slightly poorer reliability than spatially interpolated telemetric rain gauge data and significantly higher reliability than satellite estimates.
5. Short links (generally with higher frequencies) are more likely to provide less reliable precipitation estimates. On the other hand, these links are most often used in larger urban centres and would be very beneficial for precipitation estimation with high spatial resolution, which is crucial for such areas. Longer links are much more likely to underestimate the estimated precipitation. Consequently, quality control procedures for the adjustment of these data to observations from rain gauges included in the national meteorological network will be necessary.

These conclusions were deduced from the analyses conducted on a limited data set, so they cannot be treated as general.

Summarizing, from the point of view of operational usage, the estimation of CML-based precipitation may bring some potential to the issue of improving precipitation field estimation with a high temporal and spatial resolution. Already at this stage, they have a significantly higher reliability than real-time satellite estimates (Tables 2–4), and in the case of half-hourly data, it is close to the reliability of rain gauge data (Table 4).

However, the use of these estimates requires further work, among which analysis related to the bias of CML precipitation should be mentioned. Here, a change of the WAA corrections may bring some benefits to the CML precipitation reliability. This is mainly referring to short links, as they experience the largest bias due to WAA and, on the other hand, represent the huge share of CMLs in dense urban environments, where additional data are especially needed due to the unavailability of good quality radar data. Since adapted method for WAA correction may lead to the biases in quantitative precipitation estimates (Pastorek et al., 2022), this issue should be further considered as there are number of various WAA corrections, including those that rely on using constant offsets (Overeem et al., 2011). However, it is a real challenge to choose a method that works for many types of CMLs with different antennas.

Identifying sources of errors in CML data and developing effective methods for their quality control (QC), including correction and evaluation of their uncertainties, is of major importance here. Specifically, the work on quality control methodology should be carried out on a bigger data set. It is crucial from the point of view of using these estimates in algorithms for combining precipitation data from different sources in such a way that, despite the significant limitations of CML-based data, they can be applied to improve the final precipitation field estimates.

Based on the work described in this paper and the evaluation of the results obtained, general directions have been set for further work on the issues addressed here:

1. In this paper, we discussed the preliminary results of analyses of usefulness of precipitation estimated from CML data in Poland for real-time uses. The results indicate the needs for the refinement of algorithms for processing CML data for local link characteristics. Presented results will constitute the basis for further works on the use of these data, also for operational purposes.
2. It is planned to tailor the RainGaugeQC system (Ośródka et al., 2022) for quality control of CML-based precipitation data (i.e., virtual rain gauges). In this system, a quality index (*QI*) is determined for each rain gauge using several different algorithms, such as (i) comparison of the time series of rain gauge data with the time series of radar data in terms of correlation coefficient and bias and (ii) analysis of the consistency of the rain gauge data in a certain neighbourhood taking into account the magnitude of the differences from the radar measurements. The above algorithms will allow more effective detection of erroneous estimates.
3. Further works will be carried out towards combining these data with data from standard measurement techniques, primarily rain gauge and weather radar networks as well as satellite data.
4. The challenge is to validate the proposed solutions, as the true rainfall (so called: ground truth) to be used as a benchmark for the proposed methods is not known. Therefore, a methodology for this validation will be developed based on a benchmarking and interdependence analysis of different precipitation estimates.

AUTHOR CONTRIBUTIONS

Magdalena Pasierb: Conceptualization (equal); data curation (equal); formal analysis (equal); investigation (equal); methodology (supporting); validation (equal); writing – review and editing (supporting). **Zofia Bałdysz:** Conceptualization (equal); data curation (equal); formal analysis (equal); investigation (equal); methodology (equal); writing – review and editing (equal). **Jan Szturc:** Conceptualization (equal); formal analysis (equal);

investigation (equal); methodology (equal); writing – original draft (lead); writing – review and editing (equal). **Grzegorz Nykiel:** Conceptualization (equal); data curation (lead); formal analysis (equal); investigation (equal); methodology (supporting); software (equal); writing – review and editing (supporting). **Anna Jurczyk:** Conceptualization (equal); data curation (equal); formal analysis (equal); investigation (equal); methodology (lead); software (equal); validation (equal); writing – review and editing (equal). **Katarzyna Ośródka:** Conceptualization (equal); data curation (equal); formal analysis (equal); investigation (equal); methodology (equal); software (equal); validation (equal); writing – review and editing (equal). **Mariusz Figurski:** Conceptualization (equal); data curation (lead); resources (lead). **Marcin Wojtczak:** Data curation (lead); resources (equal); supervision (equal). **Cezary Wojtkowski:** Data curation (equal); resources (equal); supervision (equal).

ACKNOWLEDGEMENTS

This study is based upon work related to COST Action CA20136 "OPENSENSE" supported by COST – European Cooperation in Science and Technology.

DATA AVAILABILITY STATEMENT

The data that support the findings of this study are available from the corresponding author upon reasonable request.

ORCID

Magdalena Pasierb https://orcid.org/0000-0003-0674-429X
Zofia Bałdysz https://orcid.org/0000-0002-8398-6703
Jan Szturc https://orcid.org/0000-0001-6943-2352
Grzegorz Nykiel https://orcid.org/0000-0002-6827-0205
Anna Jurczyk https://orcid.org/0000-0003-2166-022X
Katarzyna Ośródka https://orcid.org/0000-0001-5591-4676
Mariusz Figurski https://orcid.org/0000-0001-9602-5007

REFERENCES

Atlas, D. & Ulbrich, C.W. (1977) Path- and area-integrated rainfall measurement by microwave attenuation in the 1–3 Cm band. *Journal of Applied Meteorology and Climatology*, 16(12), 1322–1331. Available from: https://doi.org/10.1175/1520-0450(1977)016%3c1322:PAAIRM%3e2.0.CO;2

Berne, A. & Uijlenhoet, R. (2007) Path-averaged rainfall estimation using microwave links: uncertainty due to spatial rainfall variability. *Geophysical Research Letters*, 34(7), L07403. Available from: https://doi.org/10.1029/2007GL029409

Blevis, B. (1965) Losses due to rain on Radomes and antenna reflecting surfaces. *IEEE Transactions on Antennas and Propagation*, 13(1), 175–176. Available from: https://doi.org/10.1109/TAP.1965.1138384

Cherkassky, D., Ostrometzky, J. & Messer, H. (2014) Precipitation classification using measurements from commercial microwave links. *IEEE Transactions on Geoscience and Remote Sensing*, 52(5), 2350–2356. Available from: https://doi.org/10.1109/TGRS.2013.2259832

Chwala, C., Gmeiner, A., Qiu, W., Hipp, S., Nienaber, D., Siart, U. et al. (2012) Precipitation observation using microwave backhaul links in the alpine and pre-alpine region of southern Germany. *Hydrology and Earth System Sciences*, 16(8), 2647–2661. Available from: https://doi.org/10.5194/hess-16-2647-2012

Chwala, C. & Kunstmann, H. (2019) Commercial microwave link networks for rainfall observation: assessment of the current status and future challenges. *WIREs Water*, 6(2), e1337. Available from: https://doi.org/10.1002/wat2.1337

Cornwall, W. (2016) Efforts to link climate change to severe weather gain ground. *Science*, 351(6279), 1249–1250. Available from: https://doi.org/10.1126/science.351.6279.1249

David, N., Alpert, P. & Messer, H. (2009) Technical note: novel method for water vapour monitoring using wireless communication networks measurements. *Atmospheric Chemistry and Physics*, 9(7), 2413–2418. Available from: https://doi.org/10.5194/acp-9-2413-2009

de Vos, L.W., Overeem, A., Leijnse, H. & Uijlenhoet, R. (2019) Rainfall estimation accuracy of a Nationwide instantaneously sampling commercial microwave link network: error dependency on known characteristics. *Journal of Atmospheric and Oceanic Technology*, 36(7), 1267–1283. Available from: https://doi.org/10.1175/JTECH-D-18-0197.1

Fencl, M., Dohnal, M. & Bareš, V. (2021) Retrieving water vapor from an E-band microwave link with an empirical model not requiring in situ calibration. *Earth and Space Science*, 8(11), e2021EA001911. Available from: https://doi.org/10.1029/2021EA001911

Fencl, M., Dohnal, M., Rieckermann, J. & Bareš, V. (2017) Gauge-adjusted rainfall estimates from commercial microwave links. *Hydrology and Earth System Sciences*, 21(1), 617–634. Available from: https://doi.org/10.5194/hess-21-617-2017

Fencl, M., Dohnal, M., Valtr, P., Grabner, M. & Bareš, V. (2020) Atmospheric observations with E-band microwave links – challenges and opportunities. *Atmospheric Measurement Techniques*, 13(12), 6559–6578. Available from: https://doi.org/10.5194/amt-13-6559-2020

Fencl, M., Valtr, P., Kvičera, M. & Bareš, V. (2019) Quantifying wet antenna attenuation in 38-GHz commercial microwave links of cellular backhaul. *IEEE Geoscience and Remote Sensing Letters*, 16(4), 514–518. Available from: https://doi.org/10.1109/LGRS.2018.2876696

Graf, M., Chwala, C., Polz, J. & Kunstmann, H. (2020) Rainfall estimation from a German-wide commercial microwave link network: optimized processing and validation for 1 year of data. *Hydrology and Earth System Sciences*, 24(6), 2931–2950. Available from: https://doi.org/10.5194/hess-24-2931-2020

Graf, M., El Hachem, A., Eisele, M., Seidel, J., Chwala, C., Kunstmann, H. et al. (2021) Rainfall estimates from opportunistic sensors in Germany across Spatio-temporal scales. *Journal of Hydrology: Regional Studies*, 37(October), 100883. Available from: https://doi.org/10.1016/j.ejrh.2021.100883

Herring, S.C., Christidis, N., Hoell, A., Kossin, J.P., Schreck, C.J. & Stott, P.A. (2018) Explaining extreme events of 2016 from a climate perspective. *Bulletin of the American Meteorological Society*, 99(1), S1–S157. Available from: https://doi.org/10.1175/bams-explainingextremeevents2016.1

Hoffmann, M., Schwartengräber, R., Wessolek, G. & Peters, A. (2016) Comparison of simple rain gauge measurements with precision Lysimeter data. *Atmospheric Research*, 174-175(June), 120–123. Available from: https://doi.org/10.1016/j.atmosres.2016.01.016

ITU-R. (2005) Specific attenuation model for rain for use in prediction methods (recommendation P.838–3). https://www.itu.int/rec/R-REC-P.838-3-200503-I/en [Accessed 17th February 2023]

Jurczyk, A., Ośródka, K., Szturc, J., Pasierb, M. & Kurcz, A. (2023) Long-term multi-source precipitation estimation with high resolution (RainGRS Clim). *Atmospheric Measurement Techniques*, 16(17), 4067–4079. Available from: https://doi.org/10.5194/amt-16-4067-2023

Jurczyk, A., Szturc, J. & Ośródka, K. (2020) Quality-based compositing of weather radar derived precipitation. *Meteorological Applications*, 27(1), e1812. Available from: https://doi.org/10.1002/met.1812

Jurczyk, A., Szturc, J., Otop, I., Ośródka, K. & Struzik, P. (2020) Quality-based combination of multi-source precipitation data. *Remote Sensing*, 12(11), 1709. Available from: https://doi.org/10.3390/rs12111709

Leijnse, H., Uijlenhoet, R. & Stricker, J.N.M. (2007) Rainfall measurement using radio links from cellular communication networks. *Water Resources Research*, 43(3), W03201. Available from: https://doi.org/10.1029/2006WR005631

Messer, H. (2007) Rainfall monitoring using cellular networks [in the spotlight]. *IEEE Signal Processing Magazine*, 24(3), 142–144. Available from: https://doi.org/10.1109/MSP.2007.361621

Messer, H. & Sendik, O. (2015) A new approach to precipitation monitoring: a critical survey of existing technologies and challenges. *IEEE Signal Processing Magazine*, 32(3), 110–122. Available from: https://doi.org/10.1109/MSP.2014.2309705

Olsen, R., Rogers, D. & Hodge, D. (1978) The aR^b relation in the calculation of rain attenuation. *IEEE Transactions on Antennas and Propagation*, 26(2), 318–329. Available from: https://doi.org/10.1109/TAP.1978.1141845

Ośródka, K., Otop, I. & Szturc, J. (2022) Automatic quality control of telemetric rain gauge data providing quantitative quality information (RainGaugeQC). *Atmospheric Measurement Techniques*, 15(19), 5581–5597. Available from: https://doi.org/10.5194/amt-15-5581-2022

Ośródka, K. & Szturc, J. (2022) Improvement in algorithms for quality control of weather radar data (RADVOL-QC system). *Atmospheric Measurement Techniques*, 15(2), 261–277. Available from: https://doi.org/10.5194/amt-15-261-2022

Ośródka, K., Szturc, J. & Jurczyk, A. (2014) Chain of data quality algorithms for 3-D single-polarization radar reflectivity (RADVOL-QC system). *Meteorological Applications*, 21(2), 256–270. Available from: https://doi.org/10.1002/met.1323

Ostrometzky, J. & Eshel, A. (2018) Empirical study of the quantization induced bias in commercial microwave Links' min/max attenuation measurements for rain monitoring. *Environments*, 5(7), 80. Available from: https://doi.org/10.3390/environments5070080

Overeem, A., Leijnse, H. & Uijlenhoet, R. (2011) Measuring urban rainfall using microwave links from commercial cellular communication networks. *Water Resources Research*, 47, W12505. Available from: https://doi.org/10.1029/2010WR010350

Overeem, A., Leijnse, H. & Uijlenhoet, R. (2013) Country-wide rainfall maps from cellular communication networks. *Proceedings of the National Academy of Sciences*, 110(8), 2741–2745. Available from: https://doi.org/10.1073/pnas.1217961110

Overeem, A., Leijnse, H. & Uijlenhoet, R. (2016a) Two and a half years of country-wide rainfall maps using radio links from commercial cellular telecommunication networks. *Water Resources Research*, 52(10), 8039–8065. Available from: https://doi.org/10.1002/2016WR019412

Overeem, A., Leijnse, H. & Uijlenhoet, R. (2016b) Retrieval algorithm for rainfall mapping from microwave links in a cellular communication network. *Atmospheric Measurement Techniques*, 9(5), 2425–2444. Available from: https://doi.org/10.5194/amt-9-2425-2016

Pastorek, J., Fencl, M. & Bareš, V. (2023) Uncertainties in discharge predictions based on microwave link rainfall estimates in a small Urban catchment. *Journal of Hydrology*, 617(February), 129051. Available from: https://doi.org/10.1016/j.jhydrol.2022.129051

Pastorek, J., Fencl, M., Rieckermann, J. & Bareš, V. (2022) Precipitation estimates from commercial microwave links: practical approaches to wet-antenna correction. *IEEE Transactions on Geoscience and Remote Sensing*, 60: 4104409, 1–9. Available from: https://doi.org/10.1109/TGRS.2021.3110004

Rahimi, A.R., Holt, A.R., Upton, G.J.G. & Cummings, R.J. (2003) Use of dual-frequency microwave links for measuring path-averaged rainfall. *Journal of Geophysical Research-Atmospheres*, 108(D15), 4467. Available from: https://doi.org/10.1029/2002JD003202

Rios Gaona, M.F., Overeem, A., Raupach, T.H., Leijnse, H. & Uijlenhoet, R. (2018) Rainfall retrieval with commercial microwave links in São Paulo, Brazil. *Atmospheric Measurement Techniques*, 11(7), 4465–4476. Available from: https://doi.org/10.5194/amt-11-4465-2018

Roversi, G., Alberoni, P.P., Fornasiero, A. & Porcù, F. (2020) Commercial microwave links as a tool for operational rainfall monitoring in northern Italy. *Atmospheric Measurement Techniques*, 13(11), 5779–5797. Available from: https://doi.org/10.5194/amt-13-5779-2020

Schleiss, M. & Berne, A. (2010) Identification of dry and rainy periods using telecommunication microwave links. *IEEE Geoscience and Remote Sensing Letters*, 7(3), 611–615. Available from: https://doi.org/10.1109/LGRS.2010.2043052

Schleiss, M., Rieckermann, J. & Berne, A. (2013) Quantification and modeling of wet-antenna attenuation for commercial microwave links. *IEEE Geoscience Remote Sensing Letteers*, 10, 1195–1199. Available from: https://doi.org/10.1109/LGRS.2012.2236074

Segovia-Cardozo, D.A., Rodríguez-Sinobas, L., Díez-Herrero, A., Zubelzu, S. & Canales-Ide, F. (2021) Understanding the mechanical biases of tipping-bucket rain gauges: a semi-analytical calibration approach. *Water*, 13(16), 2285. Available from: https://doi.org/10.3390/w13162285

Seneviratne, S.I., Nicholls, N., Easterling, D., Goodess, C.M., Kanae, S., Kossin, J. et al. (2012) Changes in climate extremes

and their impacts on the natural physical environment. In: managing the risks of extreme events and disasters to advance climate change adaptation. In: Field, C.B., Barros, V., Stocker, T.F., Qin, D., Dokken, D.J., Ebi, K.L. et al. (Eds.) *A special report of working groups I and II of the intergovernmental panel on climate change (IPCC)*. Cambridge, UK, and New York, NY, USA: Cambridge University Press, pp. 109–230.

Sokol, Z., Szturc, J., Orellana-Alvear, J., Popová, J., Jurczyk, A. & Célleri, R. (2021) The role of weather radar in rainfall estimation and its application in meteorological and hydrological modelling—a review. *Remote Sensing*, 13(3), 351. Available from: https://doi.org/10.3390/rs13030351

Uijlenhoet, R., Overeem, A. & Leijnse, H. (2018) Opportunistic remote sensing of rainfall using microwave links from cellular communication networks. *WIREs Water*, 5(4), e1289. Available from: https://doi.org/10.1002/wat2.1289

Upton, G.J.G., Holt, A.R., Cummings, R.J., Rahimi, A.R. & Goddard, J.W.F. (2005) Microwave links: the future for Urban rainfall measurement? *Atmospheric Research*, Precipitation in Urban Areas, 77(1), 300–312. Available from: https://doi.org/10.1016/j.atmosres.2004.10.009

Urban, G. & Strug, K. (2021) Evaluation of precipitation measurements obtained from different types of rain gauges. *Meteorologische Zeitschrift (Contributions to Atmospheric Sciences)*, 30(5), 445–463. Available from: https://doi.org/10.1127/metz/2021/1084

van het Schip, T.I., Overeem, A., Leijnse, H., Uijlenhoet, R., Meirink, J.F. & van Delden, A.J. (2017) Rainfall measurement using cell phone links: classification of wet and dry periods using geostationary satellites. *Hydrological Sciences Journal*, 62(9), 1343–1353. Available from: https://doi.org/10.1080/02626667.2017.1329588

van Leth, T.C., Overeem, A., Leijnse, H. & Uijlenhoet, R. (2018) A measurement campaign to assess sources of error in microwave link rainfall estimation. *Atmospheric Measurement Techniques*, 11(8), 4645–4669. Available from: https://doi.org/10.5194/amt-11-4645-2018

Wang, Z., Schleiss, M., Jaffrain, J., Berne, A. & Rieckermann, J. (2012) Using Markov switching models to infer dry and rainy periods from telecommunication microwave link signals. *Atmospheric Measurement Techniques*, 5(7), 1847–1859. Available from: https://doi.org/10.5194/amt-5-1847-2012

Wilson, J.W., Feng, Y., Chen, M. & Roberts, R.D. (2010) Nowcasting challenges during the Beijing Olympics: successes, failures, and implications for future Nowcasting systems. *Weather and Forecasting*, 25(6), 1691–1714. Available from: https://doi.org/10.1175/2010WAF2222417.1

Wolff, W., Overeem, A., Leijnse, H. & Uijlenhoet, R. (2022) Rainfall retrieval algorithm for commercial microwave links: stochastic calibration. *Atmospheric Measurement Techniques*, 15(2), 485–502. Available from: https://doi.org/10.5194/amt-15-485-2022

How to cite this article: Pasierb, M., Bałdysz, Z., Szturc, J., Nykiel, G., Jurczyk, A., Ośródka, K., Figurski, M., Wojtczak, M., & Wojtkowski, C. (2024). Application of commercial microwave links (CMLs) attenuation for quantitative estimation of precipitation. *Meteorological Applications*, *31*(3), e2218. https://doi.org/10.1002/met.2218